Formation of Pt(III) complexes in irradiated potassium tetranitroplatinate(II): a single crystal ESR study

Michel Wermeille, Michel Geoffroy* and Philippe Arrizabalaga
Département de Chimie Physique, 30 Quai Ernest Ansermet, Université de Genève, 1211 Geneva (Switzerland)

Gérald Bernardinelli
Laboratoire de Cristallographie aux Rayons X, 24 Quai Ernest Ansermet, Université de Genève, 1211 Geneva (Switzerland)

(Received April 6, 1993; revised June 2, 1993)

Abstract

X-irradiation of single crystals of $K_2[Pt(NO_2)_4]$ and of $K_2[Pt(NO_2)_4]\cdot 2H_2O$ leads to the formation of Pt(III) complexes which have been studied by EPR at 77 K. The crystal structure of the hydrated compound has been determined in order to interpret the orientation of the g and ^{195}Pt hyperfine tensors and to reassign the powder spectrum previously attributed to this compound. The nature of the trapped species is shown to be dependent upon the presence of water molecules: one of the two Pt(III) complexes formed in the hydrated crystal probably results from oxidation of the original molecule by the radiogenic $OH^{\cdot}$ radical whereas, for the second species, the water molecule seems only to participate in the stabilization of the Pt(III) complex. For the anhydrous compound this stabilizing effect is probably assured by a distant NO_2 group.

Introduction

Whereas many dimeric Pt(III) complexes have been reported in the literature [1a, 1b], monomeric Pt(III) species are very unstable and the preparation and isolation of a monomeric Pt(III) species remains exceptional [1c–g]. It is however recognized that transient Pt(III) species are often involved as reaction intermediates and the characterization of their structure is important for the elucidation of mechanisms involved in various fields of chemistry (e.g. catalysis, photochemistry, radiation chemistry, electrochemistry etc.). While pulsed radiolysis is very efficient for the detection of such species [2], ESR is certainly the most suitable technique for obtaining information about their structure. The accurate determination of the ESR tensors is however rather rare since the required measurements need that the Pt(III) species be trapped in a diamagnetic single crystal [3–7]. This explains why the g and ^{195}Pt hyperfine tensors are often estimated from frozen solutions of polycrystalline samples [8–12]; in these cases, however, it is impossible to compare the orientation of the Pt(III) complex with the crystallographic bond directions of the Pt(II) precursor: a major part of the information is lost and, in some cases, erroneous conclusions can be drawn.

*Author to whom correspondence should be addressed.

In the present article our objective is to get an insight into the role played by the molecules neighbouring a Pt(II) complex, $[Pt(NO_2)_4]^{2-}$, during its oxidation into Pt(III). The ESR spectrum of $[Pt(NO_2)_4]^{-}$ formed by radiolysis of a powder of $K_2[Pt(NO_2)_4]\cdot 2H_2O$ was reported some years ago [8]. A first attempt at obtaining the ESR tensors from the X-irradiated single crystal convinced us, however, that our results were not in agreement with those reported in the literature. Since only the crystal structure for the anhydrous compound is known [13], we first determined the crystal structure of $K_2[Pt(NO_2)_4]\cdot 2H_2O$; then we grew large single crystals of both the anhydrous and the hydrated compound and performed a careful EPR study of these two systems after X-irradiation. The results reported below explain the apparent discrepancy between the powder and the single crystal spectra and point out the crucial role that water can play in the formation process of a Pt(III) species; moreover some interactions leading to the stabilization of this unusual oxidation state of platinum are identified.

Experimental

Compounds

$K_2[Pt(NO_2)_4]$ was prepared by adding an aqueous solution of KNO_2 to an aqueous solution of K_2PtCl_4

0020-1693/93/$6.00

[14]. The anhydrous crystals were grown by slow evaporation (several days) of the reaction mixture at 30 °C. The hydrated compound $K_2[Pt(NO_2)_4]\cdot 2H_2O$ was obtained from a similar synthesis, but after a first crystallization at 20 °C, the solid compound was dissolved in water and a very slow evaporation was carried out at 20 °C. The resulting transparent crystals became rapidly (5 min) opaque when put outside the solution. This transformation was not accompanied by any change in the morphology of the crystal.

Crystal structure and ESR reference frames

The crystal structure of anhydrous $K_2[Pt(NO_2)_4]$ was published by Porai-Koshits *et al.* [13]: monoclinic $P2_1/a$, $a=7.771$, $b=12.795$, $c=9.219$ Å, $\beta=95.93°$, $Z=4$. After indexation of the faces of some selected crystals we defined an ESR reference frame where the x axis was aligned along b and where the y and z axes were coincident with a^* and c, respectively.

A crystal of $K_2[Pt(NO_2)_4]\cdot 2H_2O$ was mounted in a Lindemann capillary with the supernatant liquid to prevent degradation. The diffracted intensities were measured at room temperature on a Philips PW1100 diffractometer with monochromated Mo Kα radiation ($\lambda=0.71069$ Å). The structure was solved by direct methods (MULTAN 87 [15]). Atomic scattering factors and anomalous dispersion terms were taken from the International Tables for X-ray Crystallography [16]. The hydrogen atoms of water molecules were not observed. All calculations were performed with the XTAL program [17]. Experimental data and refinement conditions are given in Table 1 and final coordinates are listed in Table 2 (according to the atom numbering of Fig. 1).

X-irradiation and ESR spectroscopy

The single crystals, mounted on a small brass cube, were irradiated at 77 K for 3 h by using a Philips tube equipped with a tungsten anticathode (30 kV, 30 mA). After irradiation they were transferred without any warming to a finger dewar and studied on a Bruker E-200D ESR spectrometer. The angular dependence of the signals, obtained by recording the spectra by steps of 10° in the three reference planes, was then analyzed by using a second-order perturbation which takes into account the electronic and nuclear Zeeman effects as well as the magnetic hyperfine interactions. An optimization program [18] was used to determine the ESR tensors giving the best fit between experimental and calculated resonance field positions. Temperature dependence of the spectra was studied by using the VT 1100 Bruker variable temperature controller.

TABLE 1. Summary of crystal data, intensity measurement and structure refinement for $K_2[Pt(NO_2)_4]\cdot 2(H_2O)$[a]

Formula	$K_2Pt(NO_2)_4(H_2O)_2$
Molecular weight	493.3
Crystal system	triclinic
Space group	$P\bar{1}$
Crystal size (mm)	$0.15\times0.15\times0.30$
a (Å)	6.5710(9)
b (Å)	7.010(1)
c (Å)	7.2915(9)
α (°)	117.62(1)
β (°)	102.867(11)
γ (°)	97.835(12)
V (Å)^3	278.74(8)
Z	1
D_c (g cm^{-3})	2.94
$F(000)$	228
μ (mm^{-1})	13.51
A^* min., max. [19]	3.38, 7.53
$[(\sin\theta)\lambda)_{max}$ (Å^{-1})	0.704
No. measured reflections and antireflections	3278
No. observed unique reflections	1639
Criterion for observed	$\lvert F_o\rvert > 4\sigma(F_o)$
No. parameters	80
Refinement	full matrix
Weighting scheme	$1/\sigma^2(F_o)$
Max., av. Δ/σ	0.34×10^{-2}, 0.72×10^{-3}
Max., min. $\Delta\rho$ (e Å^{-3})	4.6, −5.3
S	2.62
R, R_w (%)	5.0, 3.9

[a]The cell parameters were determined by least-squares refinement on 23 reflections with $29<2\theta<42°$.

TABLE 2. Atomic coordinates and equivalent isotropic displacement parameters (Å^2) with e.s.d.s in parentheses for $K_2[Pt(NO_2)_4]\cdot 2H_2O$

	x/a	y/b	z/c	U_{eq}[a]
Pt	1/2	1/2	1/2	0.0220(2)
K	0.1757(3)	0.2315(4)	0.8585(4)	0.038(1)
N(1)	0.705(1)	0.793(1)	0.621(1)	0.028(4)
O(1)	0.802(1)	0.926(2)	0.844(1)	0.042(4)
O(2)	0.719(1)	0.893(2)	0.525(2)	0.057(6)
N(2)	0.241(1)	0.622(2)	0.457(1)	0.030(4)
O(3)	0.194(1)	0.751(2)	0.608(2)	0.048(6)
O(4)	0.139(1)	0.566(2)	0.267(2)	0.048(6)
O(01)	0.383(1)	0.686(2)	−0.006(2)	0.050(6)

[a]U_{eq} is the average of eigenvalues of **U**.

Results

Crystals of $K_2[Pt(NO_2)_4]\cdot 2H_2O$

An ORTEP representation of $K_2[Pt(NO_2)_4]\cdot 2H_2O$ is shown in Fig. 1. The structure being centrosymmetric with the platinum atom located on an inversion centre (1h), the four nitrogen atoms and the platinum atoms are coplanar. The angle formed by two successive NO_2

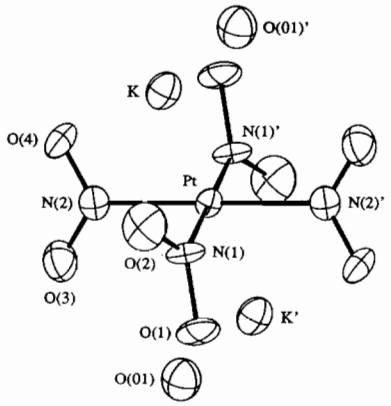

Fig. 1. ORTEP representation of $K_2[Pt(NO_2)_4]\cdot 2H_2O$. Ellipsoïds are represented with 50% probability.

TABLE 3. Selected bond lengths (Å) and bond angles (°) for $K_2[Pt(NO_2)_4\cdot 2H_2O$

Pt–N(1)	1.961(9)	K–O(4)	2.91(1)
Pt–N(2)	2.035(9)	K–O(1)	2.84(1)
N(1)–O(1)	1.37(1)	N(2)–O(3)	1.20(1)
N(1)–O(2)	1.20(2)	N(2)–O(4)	1.23(1)
N(1)–Pt–N(2)	91.6(4)	Pt–N(2)–O(3)	121.8(8)
N(1)–Pt–N(2)'	88.4(4)	Pt–N(2)–O(4)	117.2(7)
Pt–N(1)–O(1)	119.3(8)	O(1)–N(1)–O(2)	113.5(9)
Pt–N(1)–O(2)	125.0(6)	O(3)–N(2)–O(4)	121(1)

planes is equal to 70(2)°. The dihedral angles θ between the coordination plane and the NO_2 groups are equal to 71(1)°. It should be noted that although all dihedral θ angles have the same value, the structure is not helical. The shortest Pt...O(water) distance is equal to 3.52 Å and indicates that the metal atom is not coordinated to an H_2O molecule (in $K[Pt(NO_2)_4(NO)(H_2O_2)]H_2O$, the Pt...O(coordinated water) distance is equal to 2.1 Å [20]). Some selected bond distances and bond angles are given in Table 3.

In order to prevent any alteration of the crystal selected for the ESR study during indexation of its faces, the large single crystal was coated with transparent nail polish before measurement on the diffractometer, then it was irradiated at 77 K and studied by ESR (a blank experiment showed that irradiated nail polish did not produce any ESR signal). The mutual orientation of the ESR reference axes and crystallographic axes is given as follows: the columns of the matrix which transforms the fractional crystallographic coordinates into the Cartesian coordinates expressed in the ESR reference frame are (−1.4240, −4.0963, 4.98854), (−3.5972, −3.3022, −5.2338), (7.3050, −0.2675, −0.1368), respectively.

The ESR spectrum shown in Fig. 2 was recorded at 77 K with a single crystal of $K_2[Pt(NO_2)_4]\cdot 2H_2O$ freshly irradiated at 77 K. Three sets of signals are detected:

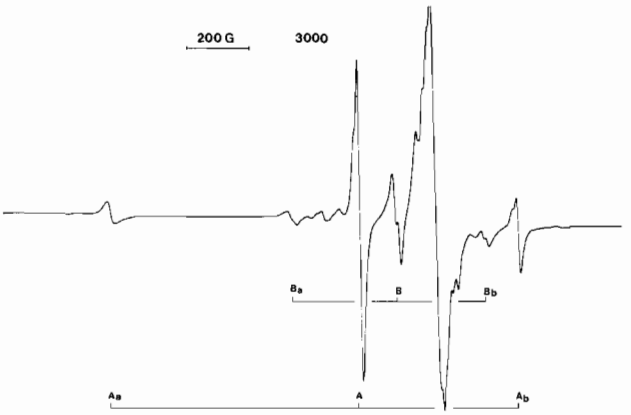

Fig. 2. Example of an ESR spectrum obtained at 77 K with an X-irradiated single crystal of $K_2[Pt(NO_2)_4]\cdot 2H_2O$.

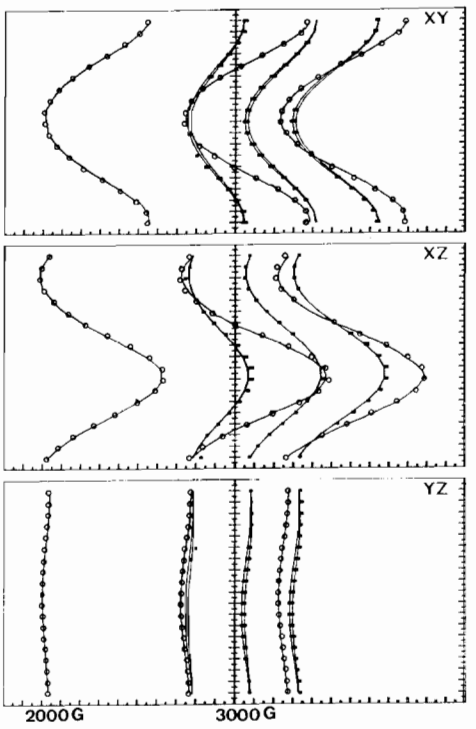

Fig. 3. Angular variation of the A (○) and B (□) ESR signals obtained with an X-irradiated single crystal of $K_2[Pt(NO_2)_4]\cdot 2H_2O$.

(i) a signal marked A surrounded by two lines A_a and A_b of lower intensity, (ii) a signal marked B with two small satellite lines marked B_a and B_b; for some orientations of the crystal an additional splitting of these three lines is observed and is due to hyperfine coupling with an additional spin1/2 nucleus, (iii) a broad isotropic signal C centred near the g_e value. As expected for signals due to a transition metal complex the A and B peaks are very anisotropic and the intensity of the satellite lines (A_a, A_b and B_a, B_b) are consistent with transitions duc to hyperfine interaction with the ^{195}Pt isotope (^{195}Pt: natural abundance = 33.8%, $I = 1/2$). This

interpretation is in accordance with the angular variation of the two sets of signals A and B shown in Fig. 3. In the YZ plane, the low field transitions B_a are hidden by the intense A lines; nevertheless, since the B and B_b signals are observed, the g and ^{195}Pt coupling tensors can be obtained. The temperature dependence of the ESR signals shows that the intensities of the A, A_a and A_b lines decrease between 100 and 260 K (vanishing temperature) whereas the intensities of the B, B_a and B_b lines increase up to 240 K and decrease up to 280 K (vanishing temperature). The signals C disappear above room temperature. The analysis of the angular variation of the ESR lines (Fig. 3) leads to the g and hyperfine coupling tensors given in Table 4.

Crystals of $K_2[Pt(NO_2)_4]$

A typical ESR spectrum obtained at 77 K with an anhydrous crystal of $K_2[Pt(NO_2)_4]$ freshly X-irradiated under liquid nitrogen is shown in Fig. 4. Three types of signals are observed on this spectrum: (i) An intense isotropic signal, marked C, which appears near $g=2.0$; (ii) signals G1 and G2 which are very anisotropic and which exhibit satellite lines marked $G1_a$ and $G1_b$ for G1 and $G2_a$ and $G2_b$ for G2; (iii) signals P1 and P2 which also exhibit the satellite lines $P1_a$, $P1_b$ and $P2_a$, $P2_b$. The angular dependence of the signals G1, $G1_a$ and $G1_b$ (Fig. 5) as well as their relative intensities clearly show that the satellite lines $G1_a$ and $G1_b$ are due to hyperfine interaction with ^{195}Pt while the signal G1, caused by the same paramagnetic molecule, corresponds to the non-magnetic isotopes. The same analysis is also valid for the other sets of signals: G2, P1 and P2 which are respectively associated with the ^{195}Pt lines ($G2_a$, $G2_b$), ($P1_a$, $P1_b$) and ($P2_a$, $P2_b$). For several orientations of the magnetic field in the XY plane the

TABLE 4. g and hyperfine coupling tensors for paramagnetic species trapped in X-irradiated single crystals of $K_2[Pt(NO_2)_4]$ and $K_2[Pt(NO_2)_4]\cdot 2H_2O$

Species	Eigenvalues	Eigenvectors		
Anhydrous compound				
		*/a**	*/b*	*/c*
Species G	$g_1=1.911$	0.1982	±0.4528	−0.8692
	$g_2=2.567$	0.6592	±0.7171	−0.2233
	$g_3=2.620$	−0.7425	±0.5286	−0.4411
	$^{195}T_1=5219$ MHz	0.2045	±0.4447	−0.8719
	$^{195}T_2=5952$ MHz	0.8392	±0.5364	−0.0767
	$^{195}T_3=6062$ MHz	−0.5018	±0.7158	−0.4833
Species P	$g_1=1.908$	−0.26074	±0.5003	−0.8256
	$g_2=2.568$	−0.8416	±0.5303	−0.0561
	$g_3=2.627$	−0.4657	±0.6800	0.5597
	$^{195}T_1=5236$ MHz	−0.2865	±0.5095	−0.8112
	$^{195}T_2=5982$ MHz	−0.7239	±0.6656	−0.1607
	$^{195}T_3=6074$ MHz	−0.6224	±0.5413	0.5595
Hydrated compound				
		/x	*/y*	*/z*
Species A	$g_1=1.943$	0.9415	−0.0576	0.3322
	$g_2=2.488$	−0.0507	0.9499	0.3083
	$g_3=2.505$	0.3333	0.3071	−0.8914
	$^{195}Pt\text{-}T_1=3509$ MHz	0.9504	−0.0917	0.2971
	$^{195}Pt\text{-}T_2=4113$ MHz	−0.1567	0.6841	0.7124
	$^{195}Pt\text{-}T_3=4119$ MHz	−0.2685	−0.7236	0.6358
Species B	$g_1=1.962$	0.9458	−0.0036	0.3247
	$g_2=2.219$	0.2387	0.6857	−0.6877
	$g_3=2.237$	−0.2201	0.7280	0.6494
	$^{195}Pt\text{-}T_1=1922$ MHz	0.9560	0.0317	0.2916
	$^{195}Pt\text{-}T_2=1701$ MHz	−0.2924	0.0263	0.9560
	$^{195}Pt\text{-}T_3=1656$ MHz	0.0226	−0.9991	0.0344
	$^{1}H\text{-}T_1=13$ MHz			
	$^{1}H\text{-}T_2=14$ MHz			
	$^{1}H\text{-}T_3=50$ MHz	−0.0066	−0.9998	−0.0199

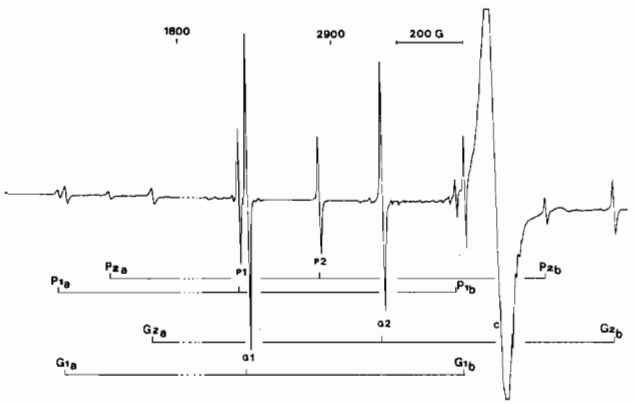

Fig. 4. Example of an ESR spectrum obtained at 77 K with an X-irradiated single crystal of $K_2[Pt(NO_2)_4]$.

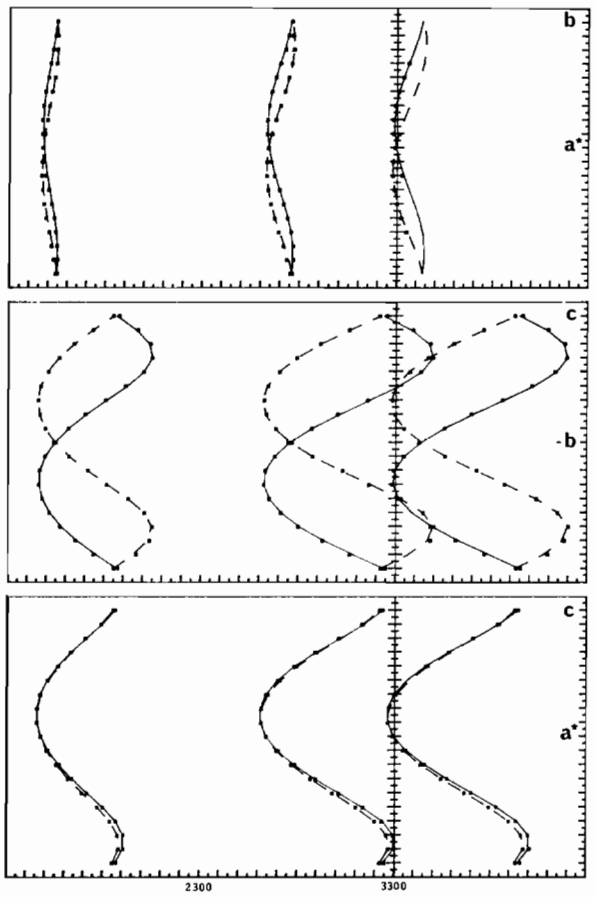

Fig. 5. Angular variation of the ESR signals G obtained with an X-irradiated single crystal of $K_2[Pt(NO_2)_4]$.

high field transitions ($P1_b$, $P2_b$, $G1_b$ and $G2_b$) are hidden by the intense C peak.

When the temperature of the crystal was slowly increased in the ESR cavity, the intensity of the signals P rapidly decreased and practically vanished at 110 K while the signals G were still detected at 160 K.

As shown in Fig. 5, the lines due to the species G1 and G2 are practically superposed in the a^*c plane as well as along the b axis and so are the signals P1 and P2. This feature, in accordance with the symmetry of the crystal, indicates that G1 and G2 are due to the same species trapped along two orientations which become equivalent along the reference axes and in the a^*c plane. The same conclusion is obtained for the P1 and P2 species.

The angular variations of the G and P signals were analyzed by using the procedure described for the hydrated compound. Due to the overlap of the lines which occurred when the magnetic field was aligned along the reference axes some ambiguity appeared when combining the various curves. This problem was solved by grinding some crystals and by irradiating the resulting powder in the same conditions as those used for the single crystals. The selected combinations of curves were those which led to sets of tensors which were the most in accord with the powder spectrum. This agreement was checked by simulating the powder spectrum with a program which sums the contribution of 150 000 orientations of the magnetic field. The resulting tensors are given in Table 4.

Discussion

In addition to free radicals formed from the ligand moiety, exposure of a Pt(II) complex to ionizing radiations is expected to generate either a Pt(I) or a Pt(III) species.

Although the g and ^{195}Pt hyperfine ESR tensors of the four species A, B, G and P do not exhibit a perfect axial symmetry, they all have $g_1 < g_2 \sim g_3$ and $(|(^{195}\text{Pt-}T_2) - (^{195}\text{Pt-}T_1)|) > (|(^{195}\text{Pt-}T_3 - ^{195}\text{Pt-}T_2)|)$ (Table 3); moreover the $\vec{g}_1$ and $^{195}\text{Pt-}\vec{T}_1$ directions are almost coincident (the $[\vec{g}_1, {}^{195}\text{Pt-}\vec{T}_1]$ angle is equal or inferior to 3° for the four species). In the axial approximation, the g tensors shown in Table 3 are characterized by $g_\parallel < g_e < g_{\perp 1} \sim g_{\perp 2}$; the ligand field theory shows that, for a d^9 species, this tensor corresponds to an axially compressed D_{4h} structure, while, for a d^7 species it corresponds to a tetragonal elongation [8, 21]. The former structure is very rare whereas the latter one has been assigned to almost all Pt(III) complexes reported in the literature [3, 5, 6, 9, 22]. Furthermore, recent MS-Xα calculations on $[Pt(NH_3)_4(OH)]^{2+}$ have shown that for a Pt–OH distance near 2 Å the unpaired electron is mainly localized in a $5d_{z^2}$ and a 6s platinum orbital [7]. The ESR parameters for a d^7 ion having a $^2A_1$ ground state have been calculated by McGarvey [23]; in C_{2v} symmetry, with the x, y axes bisecting the bond axes, the unpaired electron is localized in a $(ad_{z^2} + bd_{x^2-y^2})$ orbital and mixing with an s orbital occurs. However, the large number of unknown variables present in the spin Hamiltonian equations prevents the determination of the g and metal coupling tensors in

the general case. We have therefore assumed that only the $5d_{z^2}$ and the 6s orbitals of platinum participate in the SOMO of the ground state and have estimated the tensor elements in the axial approximation by taking only the contribution of $c_1 = \xi/(E_{dz^2} - E_{dxz})$ into account. The coefficient α takes into account the covalency effects.

$$g_{\parallel} = 2.0023 - 3c_1^2$$

$$g_{\perp} = 2.0023 - 6c_1^2 + 6c_1$$

$$T_{\parallel} = K + P_0(4\alpha^2/7 - 6c_1/7 + 15c_1^2/7)$$

$$T_{\perp} = K + P_0(-2\alpha^2/7 + 45c_1/7 - 57c_1^2/14)$$

The free ion value P_0, $g_e\beta_e g_n\beta_n \langle r^{-3} \rangle$, is obtained from the compilation of Morton and Preston (1470 MHz) [24].

Hydrated compound

Although the g and ^{195}Pt-T tensors for the A and B species are different, they all exhibit axial symmetry and their eigenvectors are almost aligned. The 'parallel' direction is expected to be aligned along the normal **n** to the PtN_4 plane; the fact that this eigenvector makes an angle of 35° with the normal to the crystallographic PtN(1)N(2)N'(1)N'(2) plane indicates that some reorientation of the anion occurred during the oxidation process. The $g_{\parallel}$ direction makes an angle of only 3° with a Pt–O(H_2O) direction and suggests that a water molecule, or a radiation product of H_2O, occupies the axial direction of a pentacoordinated Pt(III) ion. For the A species, which does not exhibit any additional hyperfine structure, it is probable that after radiogenic ionization of $[Pt(NO_2)_4]^{2-}$ the resulting Pt(III) ion is stabilized by a neighbouring water molecule, which, after migration, coordinates the metal ion. In this process the Pt...O(H_2O) distance, originally near 4.4 Å, probably decreases and some of the nitrogen atoms probably move slightly and lead to a change in the **n** direction. It is worthwhile remarking that another water molecule is present in the undamaged crystal at a shorter distance from the platinum atom (Pt...O distance = 3.52 Å), but the corresponding [$\vec{g}_{\parallel}$, $\overrightarrow{Pt...O}$] angle is equal to 47° and seems less consistent with a fifth coordination of the metal atom. As for the A species, the 'parallel' direction measured for B is aligned along a Pt...O(H_2O) direction, however the additional hyperfine coupling with a proton suggests that after migration, an ·OH radical produced by radiolysis of a water molecule reacts with a neighbouring Pt(II) ion and gives rise to the $[Pt(NO_2)_4OH]^{2-}$ species. This mechanism is reminiscent of the reaction observed in an X-irradiated single crystal of bis(ethylene diamine)platinum dihydrogenosquarate [7], where $[Pt(en)_2]^{2+}$ was oxidized by the radiogenic radical formed on the hydrogenosquarate ion. The OH group, which occupies the axial position of the square pyramid is the origin of the anisotropic proton coupling and its coordination causes a slight displacement of the nitrogen atoms.

The above mentioned equations for $g_{\parallel}$ and $g_{\perp}$ lead to slightly different values of c_1; the average value for species A and B are $c_1 = 0.115 \pm 0.025$ and $c_1 = 0.08 \pm 0.04$, respectively. For the A species, the condition $0 < \alpha^2 < 1$ implies that $T_{\parallel}$ and $T_{\perp}$ are both positive and the resulting values of α^2 and K are 0.40 and +3275 MHz, respectively. This positive Fermi contact interaction indicates a strong participation of the 6s orbital in the SOMO. If the three ^{195}Pt-coupling eigenvalues of the B species are also assumed to be positive, the values of α^2 and K calculated for this species are equal to 0.82 and 1307 MHz.

It is worthwhile mentioning that neither the A nor the B species have ESR tensors which correspond to those previously reported for an irradiated powder of $K_2[Pt(NO_2)_4] \cdot 2H_2O$.

Anhydrous compound

In order to interpret the EPR results it is necessary to recall the crystallographic results obtained by Porai-Koshits *et al.* [13] from an X-ray diffraction study. The salient feature of this structure is the existence of two independent $[Pt(NO_2)]_4^{2-}$ units whose mutual orientations are illustrated in Fig. 6. The platinum atom of each unit (respectively marked Pt(1) and Pt(2)) is placed

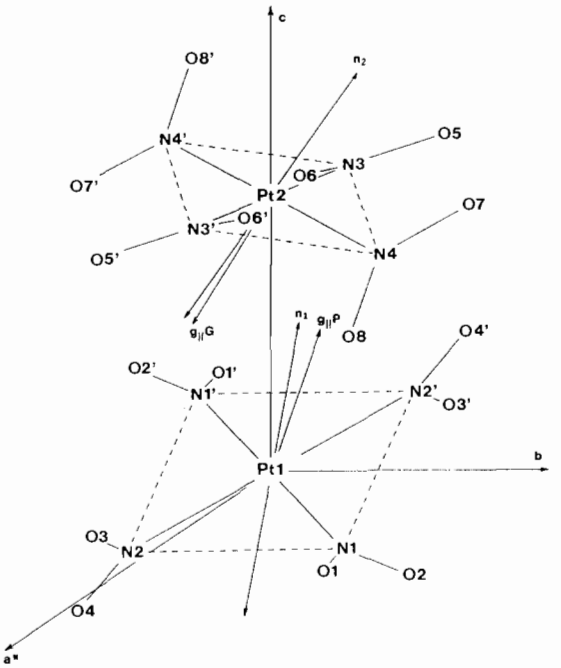

Fig. 6. Mutual orientation of the $g_{\parallel}$ eigenvectors (species P and G) and of the bond directions in an anhydrous crystal of $K_2[Pt(NO_2)_4]$.

TABLE 5. Orientation of the $g_{\parallel}$ eigenvectors in an anhydrous single crystal of $K_2[Pt(NO_2)_4]$

	$g_{\parallel}$ (Species G)	$g_{\parallel}$ (Species P)
$\mathbf{n}_1(\perp Pt(1)N_4)$	32°	8°
$\mathbf{n}_2(\perp Pt(2)N_4)$	6°	33°
Pt(2)...O'(2) (NO_2 bound to Pt(1))	13°	20°
Pt(1)---O(8) (NO_2 bound to Pt(2))	27°	5°

on the c axis and is located at the centre of the square formed by the four nitrogen atoms. The normal $\mathbf{n}_1$ to the N(1)–Pt(1)–N(2) plane, and the normal $\mathbf{n}_2$ to the N(3)–Pt(2)–N(4) plane make an ($\mathbf{n}_1$, $\mathbf{n}_2$) angle equal to 38.5°. All the $PtNO_2$ fragments are planar, but the dihedral angles between the nitro planes and the coordination plane in the first unit (48.5 and 85.8°) are different from those measured for the second unit (39.8 and 67.1°).

The similarity in the g and hyperfine eigenvalues found for the G and P species (Table 4) indicates that these two species probably correspond to the same chemical structure. Examination of the eigenvectors shows, however, that these two paramagnetic species are differently oriented in the crystal matrix. This observation is consistent with the presence of two independent $[Pt(NO_2)]_4^{2-}$ molecules in the cell and the slight differences in the ESR parameters and in the temperature dependence of the spectra probably reflect the small structural differences mentioned for the two platinate ions. Although it is impossible to unambiguously attribute the P (or G) signals to the unit containing Pt(1) or to that containing Pt(2), we will try to describe the trapped species by using the tensors given in Table 4.

In Table 5, we show the angles formed by the $g_{\parallel}$ eigenvectors of the G and P species with some directions obtained from the crystal structure. The normal $\mathbf{n}_1$ to the $Pt(1)N_4$ plane makes an angle of only 8° with the $g_{\parallel}$ direction of the P species, while the normal $\mathbf{n}_2$ to the $Pt(2)N_4$ plane makes an angle of only 6° with the $g_{\parallel}$ direction of the G species. This alignment of the g and $\mathbf{n}$ directions is consistent with the oxidation of the two types of $[Pt(NO_2)]_4^{2-}$ complexes present in the crystal and with the trapping, without any drastic reorientation, of two Pt(III) complexes with a $(d_{z^2})^1$ configuration. The stability of a tetracoordinated Pt(III) species is expected to be very low, and we have examined the possibility of a fifth coordination in axial position. The angular properties reported in Table 4 show that each $g_{\parallel}$ direction is oriented toward the oxygen atom of an NO_2 group of the neighbour dianion. Although the corresponding interatomic distance Pt...O is long (3.4 Å), this is the shortest intermolecular platinum–oxygen distance measured in the crystal structure. It is impossible to know if this NO_2 group only contributes to the stabilization of an already formed Pt(III) complex or if it directly participates in the oxidation process (e.g. via the well-known radiogenic radical NO_2). However, the absence of any ^{14}N hyperfine coupling makes improbable any appreciable spin delocalization onto a fifth NO_2 group.

The average value of c_1 calculated from $g_{\parallel}$ and $g_{\perp}$ is equal to 0.14 ± 0.03. Only positive hyperfine eigenvalues lead to an α value which verifies $0 < \alpha^2 < 1$ and the corresponding α^2 value ($\alpha^2 = 0.42$) implies a K value close to 4980 MHz. This positive Fermi contact interaction corresponds to considerable participation of a 6s orbital. The g values obtained for the G and P species trapped in the anhydrous crystal correspond, in fact, to the data previously reported for the hydrated compound. We have confirmed this point by recording the ESR spectrum obtained with an anhydrous powder of $K_2[Pt(NO_2)_4]$; it illustrates the fact that, in absence of protection, hydrated crystals spontaneously lose water molecules.

Conclusions

The present single study shows that two slightly different Pt(III) complexes are formed in the X-irradiated anhydrous compound. These two $[Pt(NO_2)_4]^-$ complexes, exhibit an unusually large K value and seem to be stabilized by the presence of a distant NO_2 group. A similar situation is observed with the hydrated crystal where a distant H_2O molecule is probably located in axial position. In this latter crystal, however, oxidation by a radiogenic OH radical also occurs and gives rise to $[Pt(NO_2)_4(OH)]^{2-}$.

Supplementary material

Tables of complete distances, bond angles, torsion angles, atomic displacements parameters and factor structure can be obtained on request from author G.B.

Acknowledgement

The financial support of the Swiss National Science Foundation is gratefully acknowledged.

References

1 (a) Chi-Ming Che, T.C.W. Mak, V.M. Miskowski and H.B. Gray, *J. Am. Chem. Soc., 108* (1986) 7840; (b) F.A. Cotton, L.R. Falvello and S. Han, *Inorg. Chem., 21* (1982) 1710; (c) R. Uson, J. Fornies, M. Thomas, B. Menjon, R. Bau, K. Sunkel and E. Kuwabara, *Organometallics, 5* (1986) 1576; (d) A.J. Blake, R.O. Gould, A.J. Holder, T.I. Hyde, A.J. Lavery, M.O. Odulate and M. Schröder, *J. Chem. Soc., Chem. Commun.,* (1987) 118; (e) R. Uson, J. Fornies, M. Tomas, B. Menjon, K. Sünkel and R. Bau, *J. Chem. Soc., Chem. Commun.,* (1984) 75; (f) H.A. Boucher, G.A. Lawrance, P.A. Lay, A.M. Sargeson, A.M. Bond, D.F. Sangster and J.C. Sullivan, *J. Am. Chem. Soc., 105* (1983) 4652; (g) H. Endres, H.J. Keller, H. van de Sand and Vu Dong, *Z. Naturforsch., Teil B, 33* (1978) 849.

2 W.L. Waltz, J. Lillie, R.T. Walters and R.J. Woods, *Inorg. Chem., 19* (1980) 3284.

3 T. Krigas and M.T. Rogers, *J. Chem. Phys., 55* (1971) 3035.

4 R. Kirmse, W. Dietzsch and B.V. Solov'ev, *J. Inorg. Nucl. Chem., 39* (1977) 1157.

5 A. Kawamori, R. Aoki and M. Yamashita, *J. Phys. C, 18* (1985) 5487.

6 F. Mehran and B.A. Scott, *Phys. Rev., 31* (1973) 99; 1347.

7 M. Geoffroy, G. Bernardinelli, P. Castan, H. Chermette, D. Deguenon, S. Nour, J. Weber and M. Wermeille, *Inorg. Chem., 31* (1992) 5056.

8 C. Amano and S. Fujiwara, *Bull. Chem. Soc. Jpn., 50* (1977) 1437.

9 T. Uemura, T. Tomohiro, K. Hayamizu and Y. Okuno, *Chem. Phys. Lett., 142* (1987) 423.

10 G.V. Nizova, M.V. Serdobov, A.T. Nikitaev and G.B. Shul'pin, *J. Organomet. Chem., 275* (1984) 139.

11 R. Vicente, J. Ribas, X. Solane, M. Font-Altaba, A. Mari, P. De Loth and P. Cassoux, *Inorg. Chim. Acta, 132* (1987) 229.

12 H. Neubacher, P. Zaplatynski, A. Haase and W. Lohmann, *Z. Naturforsch., Teil B, 34* (1979) 1015.

13 M.A. Porai-Koshits, G.A. Kukina and V.P. Nikolaev, *Koord. Khim., 4*(1978) 1435 *(Sov. J. Coord. Chem.,* (1980) 1095).

14 *Gmelins Handbuch der Anorganischen Chemie*, Platin, Teil C, Verlag Chemie, 1940, p. 166.

15 P. Mains, S.J. Fiske, S.E. Hull, L. Lessinger, G. Germain, J.-P. Declercq and M.M. Woolfson, *MULTAN*, a system of computer programs for the automatic solution of crystal structures from X-ray diffraction data, Universities of York, UK and Louvain-la-Neuve, Belgium, 1987.

16 *International Tables for X-ray Crystallography*, Vol. IV, Kynoch, Birmingham, UK, 1974.

17 S.R. Hall and J.M. Steward (eds.), *XTAL-3.0 User's Manual*, Universities of Western Australia and Maryland, 1990.

18 F. James and M. Roos, *CERN Program Library*; CERN, Geneva, Switzerland, 1976.

19 E. Blanc, D. Schwarzenbach and H.D. Flack, *J. Appl. Crystallogr., 24* (1991) 1035.

20 E.S. Peterson, R.D. Larsen and E.H. Abbott, *Inorg. Chem., 27* (1988) 3514.

21 A.H. Maki, N. Edelstein, A. Davidson and R.H. Holm, *J. Am. Chem. Soc., 86* (1964) 4580.

22 J.K. Barton, D.J. Szalda, H.N. Rabinowitz, J.V. Waszeczak, S.J. Lippart, *J. Am. Chem. Soc., 101* (1979) 1434.

23 B.R. McGarvey, *Can. J. Chem., 53* (1975) 2498.

24 J.R. Morton and K.F. Preston, *J. Magn. Reson., 30* (1978) 577.